Bifurcations and the transition to chaos in the resonant-tunneling diode

T. S. Monteiro
Department of Physics and Astronomy, University College, University of London, Gower St, London WC1E 6BT, United Kingdom

D. Delande
Laboratoire Kastler Brossel, 4 place Jussieu, Tour 12, 1er étage, F-75252 Paris Cedex 05, France

A. J. Fisher
Department of Physics and Astronomy, University College, University of London, Gower St, London WC1E 6BT, United Kingdom

G. S. Boebinger
Bell Laboratories, Lucent Technologies, 600 Mountain Avenue, Murray Hill, New Jersey 07974
(Received 20 February 1997)

Recent experiments by Muller *et al.* [Phys. Rev. Lett. **75**, 2875 (1995)] and Boebinger *et al.* [Surf. Sci. **361-362**, 742 (1996)] investigated the transition to chaos and the effects of bifurcations on the magnetotunneling spectrum of a quantum well in tilted fields. We introduce a computationally efficient model for the device which successfully reproduces the main features of the experiments. We find that a number of separate dynamical regimes in the experiment at $\theta = 11°$ are each characterized by a distinctive experimental spectral profile. We use this signature to identify a period doubling resonance and tangent bifurcation but find that the second observed period doubling in the tunneling current is not due to a bifurcation. [S0163-1829(97)01331-3]

I. INTRODUCTION

The problem of a resonant tunnelling diode (RTD) in tilted electric and magnetic fields has attracted much recent interest[1–5] as a probe of the manifestations of classical chaos in a mesoscopic quantum system. But to date, to our knowledge, it has not been demonstrated whether the experiments are amenable to *quantitative* analysis within the framework of periodic orbit theory. However, *I-V* characteristics have recently been calculated and compared with experiment.[6]

In the experiments,[1–3] spectral oscillations were found to be subject to abrupt increases in frequency. In Refs. 1 and 2, at tilt angle $\theta = 11°$, two period doublings were observed over a limited range of magnetic fields followed by a return to period-1 oscillations. The experiments in Ref. 3 were interpreted in terms of the accessibility of specific classical orbits to electrons tunneling in from the two-dimensional electron gas (2DEG) on the left of the emitter barrier. The experiments in Refs. 1 and 2, on the other hand, were interpreted as bifurcations[1,2,4] of the main traversing orbit (t_0, a two-bounce orbit) with the orbit intermittently losing, then recovering, stability as a precursor to fully chaotic dynamics.

A complete analysis within the framework of periodic orbit theory must simultaneously consider these two separate factors: a) a weighting for the accessibility of dynamical structures like periodic orbits to electrons tunneling in from the 2DEG adjacent to the emitter wall and b) another weighting by the stability parameters of the classical motion. The experiments in Refs. 1 and 2 by investigating specifically the bifurcations, were more directly concerned with changes in the classical stability.

The archetypal dynamical system used to study chaos in conservative systems with two degrees of freedom has to date been the hydrogen atom in a magnetic field.[7] The major reason why this atomic system has proved such a powerful probe of quantum chaos is that it has a scaling property which facilitates detailed quantitative comparisons with the chaotic classical motion. In other words one may ''invert'' a properly calculated scaled spectrum, by means of a Fourier transform, in order to estimate the stability parameters and amplitudes of the individual periodic-orbit oscillations.

Here we introduce two separate quantum-scaled models for the tunneling current which enable us to extract information concerning the stability and accessibility simultaneously from the amplitudes of the oscillations of the current. We also introduce a model for the current which shows that to within a global, energy-dependent envelope which is not oscillatory, the periodic orbit amplitudes are quantitatively obtained from the dynamics of an infinite well. We show by formal methods and by direct numerical comparison that to within this global envelope the model is proportional to the usual weak tunneling model.[8] Hence we demonstrate that the detailed shape of the barriers is dynamically unimportant.

We show that different dynamical regimes have a characteristic spectral line profile in the experiments at tilt angles of $\theta = 11°$ in Refs. 1 and 2. We show that the first period-doubling region is due to a bifurcation, but the second one is not. Most interestingly we show that in between the two period-doubling regions there is a further bifurcation giving rise to a ''ghost'': a contribution from a complex periodic orbit.[9] This regime is identifiable by a broad, weak sinusoidal oscillation. To date, to our knowledge, there have been no experimental studies of the characteristics of ghosts, since in the analogous atomic systems they are generally swamped by other contributions. They have, however, received considerable theoretical attention.

II. QUANTUM CHAOLOGY, PERIODIC ORBITS, AND OSCILLATIONS IN THE TUNNELING CURRENT

The literature on the quantum manifestations of classical chaos is already substantial.[10] For energy-conserving Hamiltonian systems, the most powerful theoretical framework is Gutzwiller's periodic orbit theory, which shows that where a quantum system has a chaotic classical limit, this manifests itself in a rich and subtle way in the quantum spectrum despite the fact that the quantum system shows no chaos in the sense of exponential sensitivity to perturbations.

Periodic orbit theory starts from a formulation of quantum theory as a sum over paths, each associated with a phase equal to the classical action divided by $\hbar$. In the semiclassical regime $\hbar \to 0$, i.e., where the action S is large in comparison with $\hbar$, the interferences between the various paths are mainly destructive, except in the vicinity of trajectories where the action is stationary, which selects the classical trajectories. In the chaotic limit, the typical trajectory will be one from among an infinite sea of chaotic trajectories. There are periodic orbits but these are isolated and of measure zero.

When he tried to calculate a quantum spectrum (the density of states) in the chaotic regime, Gutzwiller found that the stationary-phase approximation produces oscillatory contributions from these isolated periodic orbits. The result of this work was the Gutzwiller trace formula. The density of states $N(E)$ is given by the trace of an energy Green's function $G(q,q',E)$ for a path connecting two points q,q':

$$N(E)=\sum_i \delta(E-E_i)=-\frac{1}{\pi}\mathrm{Im}\mathrm{Tr}G. \tag{1}$$

Then, in the limit $\hbar \to 0$,

$$N(E)=N_{\mathrm{av}}(E)+N_{\mathrm{osc}}(E). \tag{2}$$

The formula gives the spectrum as a sum of oscillatory contributions $N_{\mathrm{osc}}(E)$ from periodic orbits plus a smooth background term N_{av}, called the Weyl term:

$$N_{\mathrm{osc}}(E)=\mathrm{Im}\sum_n \frac{T_n}{\pi\hbar}\sum_j \frac{\exp\left[ij\left(\frac{S_n(E)}{\hbar}-\mu_n\frac{\pi}{2}\right)\right]}{|\det(M_n^j-I)|^{1/2}}. \tag{3}$$

S_n is the action of the nth orbit, T_n its period. The index j refers to the number of traversals of the orbit. μ_n is an additional phase, the Maslov index, and M_n is the stability matrix of the unstable orbit. Detailed explanations may be found in Ref. 10.

Most notably, the trace formula relates the *quantum* spectrum to a wholly *classical* entity, the classical stability matrix M_n. Its largest eigenvalue is $\exp(\lambda T)$, where the exponent λ for an unstable orbit is the Liapunov exponent, which quantifies the exponential divergence of nearby trajectories: the characteristic signature of chaotic classical motion.

In the Gutzwiller formula, the amplitude of the contribution from a given unstable periodic orbit is in effect determined by this Liapunov exponent. So, although the quantum system exhibits no chaos in itself, the trace formula draws a beautiful connection between the quantum spectrum and the parameters of the unstable classical motion. The formula also applies to isolated stable orbits; for a stable orbit, the eigenvalues are complex quantities $i\nu T$, the winding angles of the periodic orbit.

A further challenge was in translating this framework to an experimental situation. The Gutzwiller trace formula yields the quantum density of states, from TrG. Typical experiments, however, investigated a spectrum weighted by some matrix element. Semiclassically, a quantity like TrGA would typically be involved, where A is some operator representing the appropriate observable. For the RTD, this would involve the current operator which brings in the additional relevant information, beyond the orbital stability, regarding tunneling propensities, in other words the accessibility of a given periodic orbit.

It is this experimental behavior that we seek to analyze in this work, by means of scaled quantum calculations, rather than the Gutzwiller formula itself. The semiclassical amplitudes are extracted from a quantum spectrum by means of a Fourier transform which subtracts smooth nonoscillatory contributions. This calculation is a precursor to a full analysis with a semiclassical theory.

A number of interesting questions may be addressed by an appropriate quantum calculation: In particular we wish to know where the standard periodic orbit theory fails. One well-known instance is at bifurcations. There, the weighting by the stability matrix becomes infinite, and the periodic orbit theory must be corrected appropriately.[11] Similarly, ghosts are beyond the standard semiclassical theory which gives them zero amplitude. Conclusive experimental evidence for a ghost would be a desirable objective.

III. CLASSICAL DYNAMICS AT 11°

The RTD problem comprises a quantum well with walls at $x=0$ and $x=L$, acted on by an electric field $\mathbf{F}$ along the x axis (directed toward negative x) and a magnetic field of strength B, tilted at an angle θ to $-\mathbf{F}$ in the x-z plane. The classical Hamiltonian is[3,4]

$$H=E=\frac{1}{2m}(p_x^2+p_z^2)+\frac{B^2e^2}{2m}(x\sin\theta-z\cos\theta)^2-eFx. \tag{4}$$

Below we use atomic units. Then $e=+1$ and $m\simeq 0.067$. The scaling properties of this system have been investigated for $E=0$,[4] and for general E but constant L.[5] By rescaling momenta, i.e., $\tilde{p}=p/LB$ and $\tilde{q}=q/L$, one can show that, most generally, the classical dynamics depends on the scaled energy $\mathcal{R}=E/FL$ as well as a scaled field $\rho=L/m\epsilon$ (where $\epsilon=F/B^2$) with no separate dependence on the other parameters except θ. These dimensionless parameters represent the ratio of respectively the injection energy and the diamagnetic energy inside the well to the potential energy due to the bias voltage.

In Fig. 1, we show Poincare surfaces of section (SOS) for the classical motion at four consecutive values of ρ which span the experiment. These are obtained by taking a ''slice'' of phase space at $x=0$ and plotting a point whenever a classical trajectory intersects that surface. We have selected eight

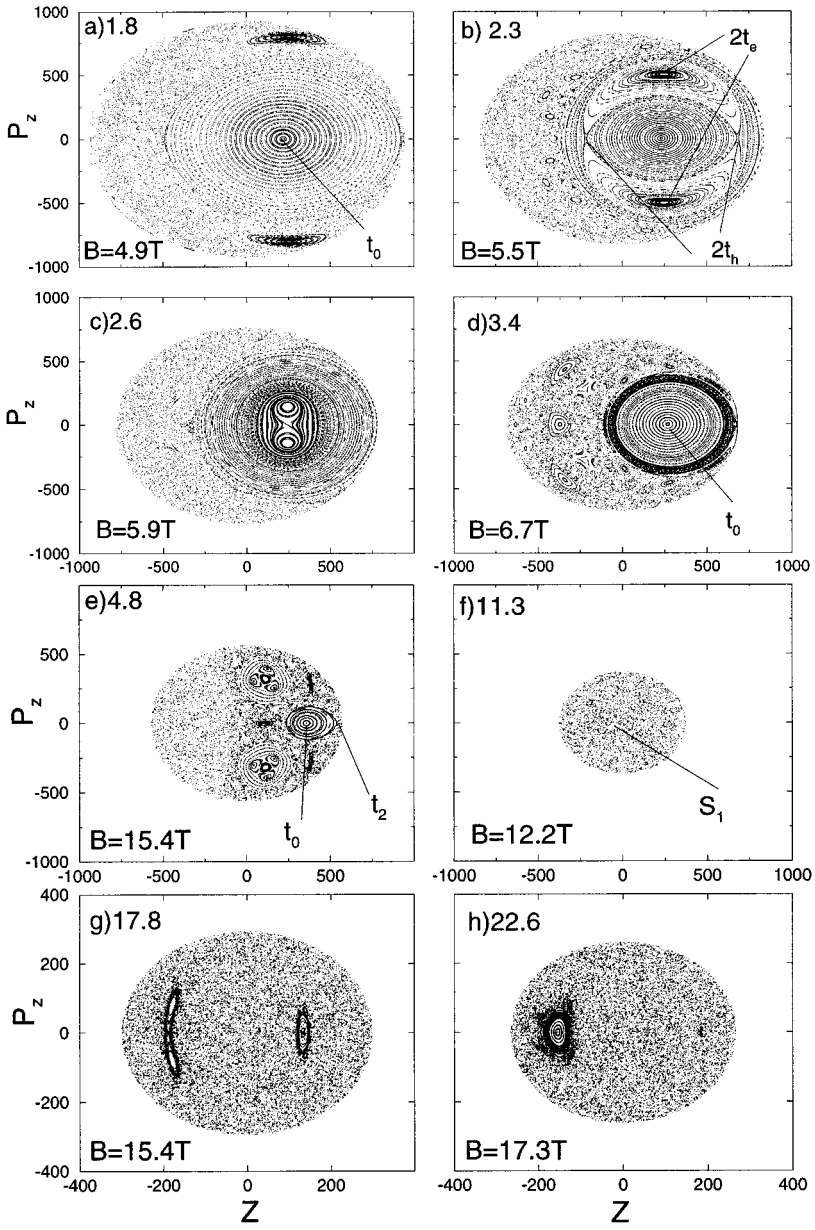

FIG. 1. Classical Poincaré surfaces of section (SOS) on the z,p_z plane calculated at the emitter $x=0$ for eight distinct classical regimes. For comparison, the magnetic field (in T) corresponding to $V=0.5$ V is shown. (a) Stable period-1 island (b) above bifurcation: period-2 island chain ($2t_e$ and $2t_h$) approaches the center (c) Period-2 bifurcation d) period-1 (e) stable orbit t_0 approaches unstable orbit t_2 prior to tangent bifurcation and appearance of ghost (f) unstable period-2 orbit S_1 most accessible to tunneling electrons (g) period-2 bifurcation (h) t_0 restabilizes. Note the change in scale for (g) and (h).

separate classical regimes corresponding to different ρ, indexed by the letters (a) to (h):

We discuss these further below, but in brief, Fig. 1 shows the following:

(a) $\rho=1.8$, where the dynamics is dominated by a large stable island, centered on a stable two-bounce period-1 periodic orbit (the t_0 orbit in Ref. 5). This is perhaps the key periodic orbit of the RTD problem, since it is predominant in the experiments for low fields.[3,5]

(b) $\rho=2.3$, where an ''island chain,'' in other words a pair of periodic orbits of double the period, approaches the central fixed point of t_0. The stable orbit (elliptic fixed point) is indicated as $2t_e$. The unstable one (hyperbolic fixed point) is denoted by $2t_h$.

(c) $\rho=2.6$, where the stable/unstable pair is absorbed at the central fixed point. First the unstable orbit is absorbed, and t_0 loses stability, then the stable orbit is absorbed and t_0 restabilizes. The whole process represents a period-2 bifurcation of the orbit t_0.

(d) $\rho=3.4$, where t_0 has restabilized once again and there is once again a period-1 stable island.

(e) $\rho=4.8$, where t_0 prepares for what is called a tangent bifurcation where it annihilates with a different, unstable, two-bounce orbit referred to below as t_2. In the SOS the fixed points of the orbits (arrowed) approach each other. When t_0 and t_2 have annihilated (this occurs at $\rho=5.2$) there will be no real period-1 periodic orbit, hence no corresponding contribution to the Gutzwiller trace formula. However, there exist two complex ''ghost'' periodic orbits which are periodic solutions of the classical equations of motion, but in a complexified phase space. These periodic orbits are born from the real period-1 orbits at the bifurcation; they will appear in the quantum spectrum as contributions which decay exponentially as $\hbar\rightarrow 0$. These are the ghosts.

(f) $\rho=11.3$ where all the orbits reaching the emitter wall are unstable. There is, however, a not-too-unstable period-3 orbit S_1,[5] which is most accessible to the tunneling electrons.

(g) $\rho=17.8$, where the orbit t_0 restabilizes by another period-2 bifurcation.

(h) $\rho=22.6$, where the orbit t_0 is centered on a small stable island giving another period-1 contribution.

Clearly the SOS also show many other smaller dynamical structures and bifurcations. The classical dynamics has structure on infinitely fine scales but only bifurcating structures comparable to phase space of area $\simeq\hbar$ should be important in the analysis of the experiment.

IV. QUANTUM DYNAMICS AT 11°

We have investigated two types of quantum spectra:

(1) A fixed B, fixed $\mathcal{R}$ spectrum

$$\left(-\frac{1}{2m}\nabla^2+\frac{(L^2B)^2}{2m}(\tilde{x}\sin\theta-\tilde{z}\cos\theta)^2\right)\psi_i=V_i(\mathcal{R}+\tilde{x})L^2\psi_i. \tag{5}$$

Here $\tilde{x}=x/L$ and $\tilde{z}=z/L$. The eigenvalue V_i is the voltage drop across the well. This corresponds closely to the experimental I-V traces, since there B is kept fixed, while the voltage is tuned from 0–1 V, $\mathcal{R}$ being kept approximately constant; here we use $V\simeq FL$. The proportionality of V and F has been established experimentally, so taking $V\simeq FL$ is not an unreasonable approximation at this point in the discussion. In the experiments, $L=120$ nm and $\mathcal{R}\simeq 0.15$.[2] This model avoids the usual requirement for separate solutions of the Hamiltonian for each change in voltage as, e.g., in Ref. 6.

(2) A fixed $\mathcal{R}$, fixed ρ spectrum

$$\left((\tilde{x}\sin\theta-\tilde{z}\cos\theta)^2-\frac{2}{\rho}(\tilde{x}+\mathcal{R})\right)\psi_i=\frac{1}{(B_iL^2)^2}\nabla^2\psi_i. \tag{6}$$

In this case, the (generalized) eigenvalues B_i are the magnetic field values. Because of the classical scaling, all states correspond to the same classical dynamics. The classical action along a trajectory $S=\int p\,dq$ becomes $S=BL^2\int\tilde{p}\,d\tilde{q}=BL^2S(\mathcal{R},\rho)$, which implies that (BL^2) plays the role of an effective Planck constant $\hbar^{-1}\simeq BL^2$. Hence, in the semiclassical limit, the effect of classical orbits appears in the spectrum (plotted as a function of B, since L is a constant) as modulations of constant frequency. These modulations can be revealed by a Fourier transform of the spectrum carried out with respect to BL^2 as peaks at the actions of the relevant classical orbits. Our Fourier transforms of the case (2) spectra were carried out with respect to principal quantum number $N=BL^2\sqrt{(2\mathcal{R}+1)/\rho}/\pi$ rather than B since $N\propto B$; the units for the scaled actions $S(\mathcal{R},\rho)$ are then more convenient since the simplest traversing orbit t_0 represents a peak in the Fourier transform close to action 1; period doubling gives a peak near 2. Physically, N roughly represents the number of oscillations along x of the wave function.

The other very important quantum number is the number of lateral oscillations n_L (i.e., in the z dimension) in the ergodic wave function (one which fills the allowed energy surface). n_L is roughly the number of Landau states supported by the energy surface on the emitter $n_L\simeq BL^2(2\mathcal{R}+1)/2\rho$; it determines the minimum area a classical phase-space structure (such as for example an island of stability) must occupy on the SOS in order to be experimentally significant. Hence the ability to resolve contributions from periodic orbits of similar action in the experiment depends strongly on n_L. This is especially important at bifurcations where two or more orbits of similar action are born together, then move apart as ρ is varied.

We solved both these equations to obtain eigenvalues of the infinite well, by expanding the eigenfunction in a basis of harmonic-oscillator states in z coordinates and functions $F_n(x)$ which can be either plane waves or Gegenbauer polynomials in the x coordinate:

$$\psi_i(x,z)=\sum_{n,l}A_{nl}F_n(x)H_l(z)\exp(-B\cos\theta z^2/2). \tag{7}$$

The current is then obtained by a sum of eigenstates weighted by their respective tunneling probabilities W_i: hence $I(V)=\Sigma_iW_i^2\delta(V-V_i)$ for the I-V characteristics or $I(B)=\Sigma_iW_i^2\delta(B-B_i)$ for a scaled spectrum. A model for the W_i is described below.

V. TUNNELING MODEL

For the RTD in tilted fields, the Bardeen transfer Hamiltonian formalism,[8] although a weak tunneling approximation, has been shown to give good agreement with experiment.[6] A full Bardeen type calculation requires detailed knowledge of the barrier heights and widths. However, if we are only interested in the *relative* intensities of the periodic orbit oscillations, we can show that the barrier shape is unimportant and the periodic orbit oscillations are quantitatively determined by the classical dynamics of the infinite well.

Below we (1) introduce a simple tunneling weight in terms of the form of the wavefunction for the infinite well, and (2) demonstrate by a theoretical argument and by direct comparisons with the Bardeen treatment, that, to within a global scaling factor, the amplitudes of oscillations obtained from our model are proportional to the usual Bardeen treatment, provided the well width is large relative to the barrier width.

The transition probability for transfer of an electron from one side of a barrier of finite height between $x=-a$ and $x=0$ to the other within the Bardeen formalism[8] is

$$P(E)=\frac{2\pi}{\hbar}\sum|\mathbf{M}_i|^2\delta(E-E_i) \tag{8}$$

and so is given in terms of a matrix element $\mathbf{M}_i$ weighting the density of final states of energy E_i. For weak tunneling, where separation of the solutions is allowable, the $\mathbf{M}_i$ are obtained in terms of ϕ_0, the solution valid to the left of $x=0$ and ψ_i the quantum solution for the eigenstates of the well and valid for $x>-a$:

$$\mathbf{M}_i=\frac{1}{2m}\left[\phi_0^*\frac{\partial\psi_i}{\partial x}-\psi_i^*\frac{\partial\phi_0}{\partial x}\right]\Bigg|_{x=x_b}\delta_{l0}. \tag{9}$$

This matrix element can be evaluated for any x and is independent of x_b provided $-a<x_b\leq 0$. But $\mathbf{M}_i$ can be evaluated arbitrarily close to $x=0$. The tunneling electrons outside the well are mostly confined to the lowest $l=0$ Landau state. This quantum number is conserved so only the $l=0$ component of the well contributes, provided $l>0$ states are negligibly populated. The initial state should be slightly displaced

relative to the origin to allow for the mean distance between the 2DEG and $x=0$. However at 11° this correction is negligible.

In the infinite barrier case, very close to the walls and hence to its node, $F_n(x)$ take a form linear in x, while the derivatives are constant for both Gegenbauer polynomials or plane waves; e.g., for a plane-wave basis $F_n(\delta) = \sin n\pi\delta/L \simeq n\pi\delta/L$, and similarly $\partial\psi_i/\partial x \simeq n\pi/L$.

We introduce a weighting W_i^2 for each eigenstate which we calculate from Eq. (9), but using the solutions of the infinite well:

$$W_i = \sum_n \frac{n\pi}{L} A_{nl=0}. \tag{10}$$

Below, we show that $W_i \propto \mathbf{M}_i$. One method for calculating $\mathbf{M}_i$ is to solve for the eigenstates of well of width L with finite barriers of width d contained inside a larger infinite well (with infinite barriers at $x=0$ and $x=L+2d$) with the requirement that d should exceed the penetration length of the wavefunction in the barriers.

For the system described above for a finite barrier of height U_b, but where $U_b \gg E$, the perturbation to the $\psi_i(x=\epsilon,z)$ and to $\partial\psi_i/\partial x(x=\epsilon)$ is smooth and weak relative to the 1200 Å infinite well. Here ϵ may be small but is not too close to the node at $x=0$ and $x=1200$ Å of the infinite well. Other than very close to the emitter where the infinite barrier wave function has a node, the eigenstates are only weakly perturbed.

Now we consider first the Bardeen matrix element with the correct (finite barrier) boundary conditions, taken with an exponentially decaying function from the left: $\phi_0 = G(E)\exp(-\gamma x)$, where $\gamma = \sqrt{2m(U_b-E)}$ and $k = \sqrt{2mE}$. For the high barrier case $\gamma \gg k$, $\psi_i = C(E)\exp(\gamma x)$ for $x \leq 0$, and $\psi_i = C(E)[1+\gamma x + O(x^2)]$ for $x>0$.

$C(E)$ and $G(E)$ are slowly-varying (non-oscillating) functions of energy. Evaluating the matrix element correctly within the barrier, we obtain

$$\mathbf{M}_{\text{Bardeen}} = 2\gamma C(E) G(E), \tag{11}$$

which is independent of x for $x \leq 0$.

We now consider the correct boundary conditions for the infinite well: $\psi_i^{\text{inf}} = 0$ for $x \leq 0$, and $\psi_i^{\text{inf}} = \alpha(E)x + O(x^3)$ for $x>0$. But since $\psi_i(\epsilon) \simeq \psi_i^{\text{inf}}(\epsilon)$, we expect that $\gamma C(E) \simeq \alpha(E)$.

We now evaluate Eq. (9), but at a point $x = +\delta < \epsilon$, *outside* but close to the barrier and hence close to the node of the wavefunction, i.e.,

$$\mathbf{M}_{\text{inf}} = \alpha(E) G(E) \simeq \mathbf{M}_{\text{Bardeen}}/2. \tag{12}$$

But from our solutions of the infinite well problem, we have $\alpha(E) = \Sigma_n (n\pi/L) A_{nl=0}$. So then we have

$$W_i = \sum_n \frac{n\pi}{L} A_{nl=0} \simeq \frac{\mathbf{M}_{\text{Bardeen}}}{2G(E)}. \tag{13}$$

Hence to within an overall non-oscillatory envelope, dependent on the initial state, our model weighting is proportional to the correct Bardeen matrix element.

In Fig. 2, we show a comparison between our model and

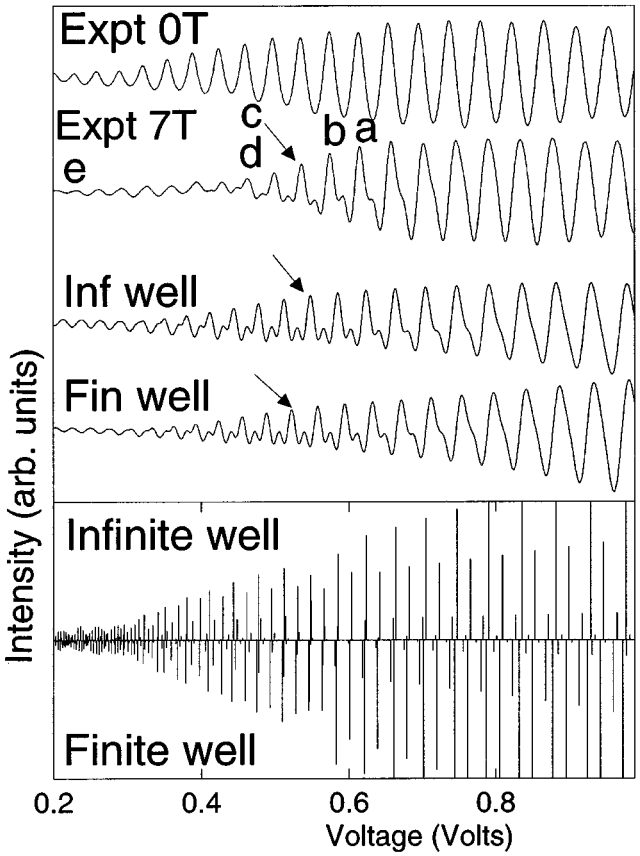

FIG. 2. Experimental I-V traces at 0 and 7 T and I-V spectra calculated at $B=6$ T showing successively the different classical regimes. The letters indicate the different dynamical regimes seen in the experiment and shown in Fig. 1: (a) and (b) torus quantization; (c) symmetric profile characteristic of the bifurcation (arrowed); (d) left-asymmetric profile below bifurcation; (e) ghost. The theoretical spectra at 6 T show both the results of our model (infinite well) as well as results using the Bardeen transfer Hamiltonian formalism. Both the theoretical stick spectra and the finite resolution spectra are shown.

a Bardeen calculation with a barrier of height 1 V and width $d=100$ a.u. of the emitter wall. The finite-barrier spectra have been rescaled by a constant factor. The finite and infinite barrier spectra are remarkably similar, especially in the case of the smoothed spectra. The main differences are in the smooth nonoscillatory envelope and in a small shift in voltage: in the finite barrier case, the electrons are accelerated by the field over the extra distance through the barrier, and enter the well with a correspondingly higher injection energy. For the purposes of comparison, the shift in voltage $\simeq Vd/L$ has been added to the unsmoothed spectra, but not to the smoothed spectra. Some individual states near avoided crossings are sensitive to the small perturbation resulting from the slight change in injection energy and in the effective width of the well. This is especially the case in the chaotic regime. However, the small perturbation leads to mixing between neighboring levels and hence to a simple redistribution of tunneling probability between close neighbors, so the smoothed spectra are unaffected. But even the unsmoothed spectra is seen to be in quite good agreement with the Bardeen calculation. This model is not appropriate for narrow well experiments where $L \simeq d$. In that case the perturba-

tion to individual levels due to the change in effective width of the well is substantial; also, the drift term $Vd/L \simeq V$.

We have also compared our model with another completely different experiment,[3] where abrupt period-doubling of the current oscillations were observed in individual I-V traces. For that system, an applied voltage of $U=0.4$ V corresponds to a voltage drop across the device of about $V=0.25$ V, so we scaled our V by a factor of 1.5. Our calculations reproduced the period-doubling observed at $U \simeq 0.35$ V as well as other features.

The effects of band nonparabolicity are sometimes corrected for by means of a voltage dependence of the effective mass $m=m(V)$.[6] We have not explicitly done this but the dynamics depends only on the product $m(V)V$, so any increase in the effective mass will manifest itself in a proportionate reduction in the calculated eigenvalue V_i. One would then simply need to rescale the V axis appropriately. Hence the I-V patterns and scaled spectra may be distorted at high voltages (stretched out) if m is increasing but any basic period doubling patterns will be unchanged.

The tunneling current has a large smooth contribution superposed on the I-V oscillations. This mirrors periodic-orbit theory where descriptions of the spectra have a smooth (Weyl) term plus periodic orbit oscillations. In the experiments in Refs. 3 and 6, this smooth background is suppressed by differentiating the current; In the Bell Lab experiments,[1,2] the background was simply subtracted. Hence in the calculations shown in Fig. 2, which are comparable with Bell Lab data, we have subtracted the nonoscillatory background. This procedure has the advantage of preserving the line profiles (to within experimental resolution) which, as discussed below, are critical in our analysis.

So, although the implementation of the full Bardeen method is numerically straightforward when U_b and d are known, our model demonstrates that a semiclassical theory based on the hard-wall scattering periodic orbits will give a quantitative description of the observed oscillations. The details of the tunneling represent a smooth envelope which, like the Weyl term of periodic-orbit theory, may be eliminated as discussed below. We have neglected the collector barrier in this instance, since we find that it does not exert a strong selective effect on the periodic orbits as they all reach the collector at high speed.

In Fig. 2, we show also experimental I-V traces.[2] Experimental resolution is limited by the lifetime for phonon emission; also, there is a voltage dependence in the spectral line width due to coupling to the continuum as $E+V$ approaches $\simeq U_b$. This is seen in the I-V trace for $B=0$ in Fig. 2.

At $B=0$, the oscillations are due to one stable straight-line periodic orbit only, so changes in the line widths and amplitudes are not due to the classical dynamics, but rather to the tunneling. Hence we use here the $B=0$ I-V traces to estimate the voltage dependence of the width. The observed width increases from 14 mV at 0.5 V to 24-mV at 1 V. We have therefore convolved the calculated spectra in Fig. 2 by a Gaussian $\exp[-(V_i-V)^2/2w^2]$ with $w=0.003+0.002(V/0.5)^{1.5}$, giving similar widths as a function of V. The letters on the $B=7$ T curves label the different classical regimes shown in the SOS in Fig. 1. Both our model and the Bardeen matrix element involve a smoothly increasing N^2 tunneling envelope, present even for $B=0$ T since in a given eigenstate the A_{nl} are peaked about $n \simeq N$. Hence in the spectra shown in the next section (Fig. 3), we find it more convenient to show a ''normalized'' current $=I(V)/N^2$. Then the normalized current for $B=0$ T corresponds to a set of period-one oscillations all of equal height.

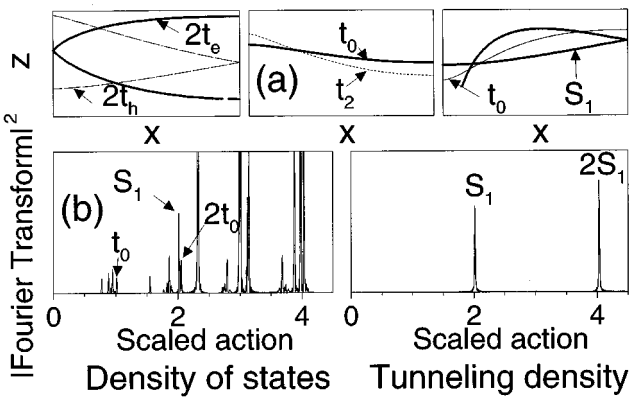

FIG. 3. (a) Shape in the x-z plane of the most important orbits showing the stable/unstable pair involved in the period doubling bifurcation $2t_h$ and $2t_e$; the t_0 and t_2 orbits which annihilate, leaving a ghost; and the S_1 orbit mostly responsible for the second period doubling. (b) Fourier transforms of the (quantum) density of states and the tunneling density for $\rho=11.28$. All the peaks correspond to periodic orbits of the classical system. While there are plenty of peaks for the density of states, the tunneling density selects only traversing orbits bouncing on the collector near $z=0$, here S_1 and its repetitions.

In sum, Fig. 2 shows that especially for the smoothed spectra there is excellent agreement between our model and the Bardeen transfer Hamiltonian formalism to within the envelope $G(E)$. The one minor difference is a small voltage shift $\simeq Vd/L$ due to the additional acceleration of the electrons in the finite barrier. For the stick spectra this shift was subtracted for the purposes of comparison.

Figure 2 also shows that our I-V spectra reproduce the detailed line shapes seen in the experiment corresponding to a succession of different classical regimes. These are discussed in detail below.

VI. QUANTUM RESULTS AND COMPARISON WITH EXPERIMENT

We can now use our *scaled* spectra to demonstrate how periodic orbits contribute differently to the density of states and the tunneling density. Only a few periodic orbits contribute to the tunneling density. For example, Fig. 3 shows a Fourier transform of the density of states and another of the tunneling current. The horizontal axis then shows peaks at the scaled actions of the important periodic orbits. While the density of states itself contains plenty of modulations at various frequencies—appearing as numerous peaks in its Fourier transform—the tunneling density at this ρ has a much simpler structure dominated by the S_1 orbit and its repetitions.

In Fig. 4, we show several *scaled* spectra for fixed $\mathcal{R},\rho$ in the range of experimental interest. Each corresponds to a particular classical regime illustrated in Fig. 1, identified by the letters (a) to (h). These may be also compared with the experimental traces in Fig. 2, which show a similar sequence of line profiles.

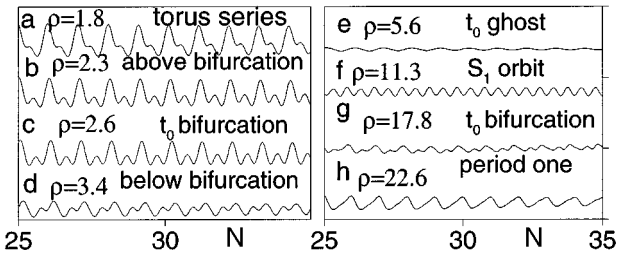

FIG. 4. Numerically calculated tunneling density spectra displaying the characteristic line profiles corresponding to the different classical regimes shown in Fig. 1. The spectra were obtained at fixed scaled field (fixed classical dynamics) taking into account the experimental finite resolution.

We can now understand the origin of both period-doubling regions observed in Refs. 1 and 2 as well as the region in between. At low ρ—spectral region (a)—the only short orbit of importance is t_0, a two-bounce orbit which at $\theta=0$ is a straight line, but which in general winds about the B field; see Fig. 3. The shorter one-bounce orbits do not contribute to the tunneling.

In regions (a) and (b), t_0 is stable and surrounded by regular invariant tori. For an isolated stable orbit[12] centered on a large elliptic island, a sum over traversals of the orbit will resolve discrete states, in fact series of harmonic-oscillator-like levels with quantization condition $\delta[S/2\pi\hbar - k - (K+\frac{1}{2})\nu/2\pi - \mu/4]$ where k represents quantization along the orbit and K perpendicular to the orbit; ν is the winding number of the orbit and μ its Maslov index. States characterized by $K=0$ are localized on the elliptic fixed point; states with higher K are localized on concentric tori. Tunneling in regions (a) and (b) is dominated by the $K=0$ and the weaker $K=1$ series. This produces a pattern of two series which are still *period-1* but are out of phase by ν. The characteristic right-asymmetric profile is seen in the experiment (Fig. 2; see also Fig. 5).

As ρ increases, t_0 moves toward its 2:1 resonance (at $\rho=2.6$), where two successive period-doubling bifurcations take place as the stable/unstable pair of orbits is absorbed: ν tends to π and the spectrum is truly period doubled. The 2:1 resonance—spectrum (c)—is easily identified by a symmetric profile, both in the calculations and the experiment. This provides an important check on the experimental parameters, since the symmetric profiles may be used to pinpoint the approximate locus of $\rho=2.6$ curve. The observed symmetric profile in fact is slightly displaced, following roughly the *linear* locus $V=0.11B-0.27$ and deviating visibly from a parabola at high voltage (B in T, V in V). Below the bifurcation, t_0 restabilizes and torus quantization yields a left-asymmetric profile [region (d)] since the $K=1$ torus now dominates the current and $K=0$ is weaker.

With increasing ρ, the stable island corresponding to t_0 progressively shrinks until t_0 merges with an unstable two-bounce orbit t_2 in a tangent bifurcation at $\rho=5.2$. This represents a new bifurcation region, not previously identified, and is especially interesting since it leaves a ''ghost'' contribution[9] for $\rho>5.2$ which decays with distance from the bifurcation. In this regime the spectrum [see Fig. 2, region (e)] is characteristic of unstable motion, with periodic level clustering rather than discrete states. The ghost has negligible harmonics, so the characteristic region (e) profile is a weak period-1 near-sinusoidal modulation, noticeably broader than the experimental broadening width. In contrast a not too unstable orbit with significant harmonics produces a Lorentzian profile. A stable orbit yields sharp peaks, as shown in Fig. 2, since its quantization, as explained above, produces discrete states. The experimental traces in Fig. 2

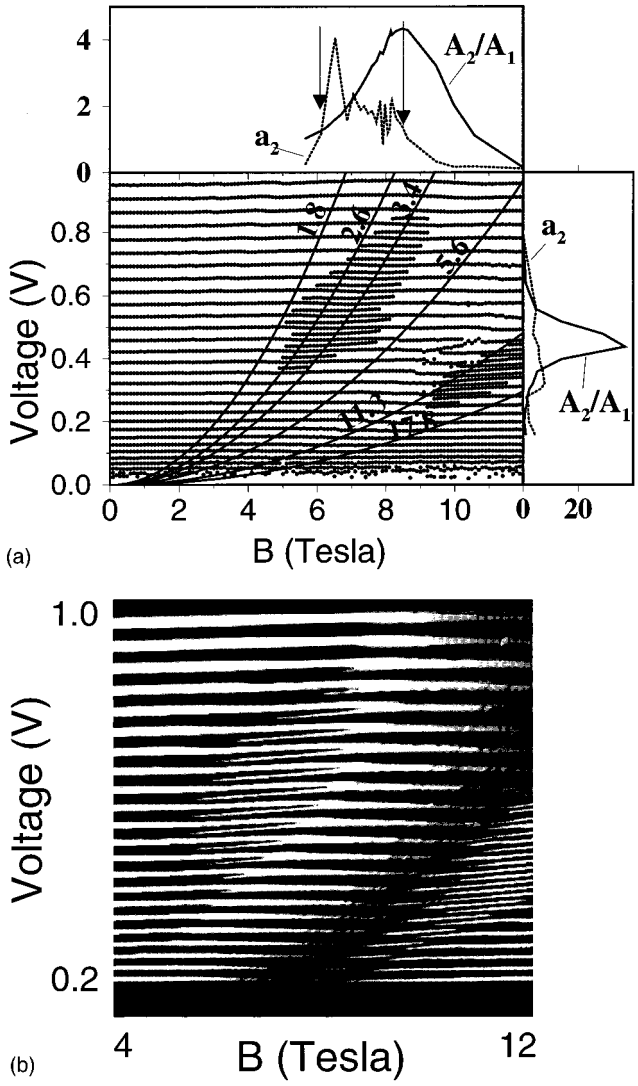

FIG. 5. (a) Comparison between experiment and period-doubling amplitudes. a_2 (broken line) represents the amplitude for the peak in the Fourier transform of the unweighted density of states near twice the action of t_0; A_2/A_1 is the ratio for the second and first traversals of t_0 in the tunneling density (density of states weighted by tunneling probability). The amplitudes are functions of ρ, but have been plotted on nonlinear scales to correspond to the parabolic curves of constant ρ (at the values used in Fig. 1) overlaid on the experimental results. The two period-doubling regions experimentally observed correspond to maxima of A_2/A_1. The first one is associated with bifurcations of t_0, while the second corresponds to a maximum contribution of the orbit S_1. (b) Density plot of the calculated current, taking into account the finite experimental resolution and its variation with the voltage which may be compared with the experiment shown in (a). The very good agreement between the two suggests that the approximation used for the tunneling density catches the essential part of the physics.

are consistent with this interpretation as may be seen by comparing experimental profiles for the ghost at $V \simeq 0.2$ at $B=7$ T with the corresponding $B=0$ T profiles near $V \simeq 0.2$ V.

The region between (e) and (f) corresponds to a fully chaotic surface of section at $x=0$: all orbits which can contribute to tunneling are unstable. Both period-1 and period-2 oscillations are quite weak; the experiments do show some irregularity within this range, just before the second period doubling. The t_0 fixed point reappears at $\rho=7.1$. It stabilizes and bifurcates again at $\rho=18.3$. Finally at $\rho=22.6$, it has restabilized, and the modulation is once again period-1 [regime (h)].

However, the period doubling in the spectrum experimentally (and numerically) observed near $\rho=11$ has a different origin. This can be *unambiguously* determined from our scaled quantum calculations. Indeed, the dominant peak in the Fourier transform occurs at the action of S_1 (2.015), *not* at the action of $2t_0$ (2.032).

To permit comparisons between semiclassical amplitudes and tunneling characteristics, we have superimposed in Fig. 5(a) lines of constant scaled field on the experimental results. We have also plotted the amplitude a_2 of the period-2 modulation (peak nearest the second traversal of t_0) for the *density of states* (broken line) as well as the ratio of the second and first traversal A_2/A_1 for the *tunneling density* (solid line). The latter gives an indication of the range where the period doubling is visible. The amplitudes were obtained from Fourier-transformed calculated spectra spanning the experimental voltage range.

For the first period doubling, a_2 shows a profile consistent with two back-to-back bifurcations, with exponential decay above about 1.5 and 2.6. The peak amplitudes occur slightly above the bifurcation points, as expected, at about 1.6 and 2.4, respectively, and the oscillating region above the two bifurcations oveRlaps and interferes. However the tunneling density shows that the first bifurcation is unimportant for the tunneling; the strong maximum at 1.6 is completely eliminated since at that point the bifurcated orbits translate into amplitude in high Landau states. The A_2/A_1 curve is in much better agreement with the experimental results.

For the second period-doubling region, a_2 shows a small maximum at about $\rho=17$, just above the period doubling bifurcation of the t_0 orbit. This bifurcation is much narrower than the one at 2.6 and has a weaker maximum. For $\rho>11$, a_2 is dominated by the amplitude of S_1 (where S_1 and $2t_0$ may be resolved in the Fourier transform, and a_2 represents the amplitude of the largest peak). The results show that the amplitude of S_1 at about $\rho=11$ is of the same order as that of $2t_0$. However the injection point of S_1 is far more favorable to tunneling, and the tunneling density shows a drastic increase in the period-doubled amplitude due to S_1, peaking at about $\rho=12.5$, with a very much weaker tail above $\rho=17$ due to $2t_0$. Hence the second period-doubling region is not related to a bifurcation of t_0, but rather to a local maximum of the contribution of S_1 to the tunneling density when this orbit's injection point is favorably fed by electrons from the ground Landau state.

This changeover between period-1 tunneling due to t_0 and higher frequency oscillations due to S-type orbits was observed in experiments carried out by Fromhold *et al.*[3] for scaled fields $\rho \simeq 17$ for $\theta > 15°$ but with $\mathcal{R} \simeq 0.2$–0.25. So it seems likely that the second period doubling here is of similar origin, with a small contribution due to the bifurcation of t_0. Finally, Fig. 5(b) shows the global spectrum of the tunneling density in the range [4T–12 T,0.2–1 V] obtained. The density of the plot represents the computed current (black regions correspond to low current, white regions to high current). We take $V=FL$. Remarkably, the figure reproduces the essential features of the experiment [compare with Fig. 5(a)]: the first period-doubling region around (7 T,0.55 V), the irregularity before the second period-doubling and the second period-doubling around (11 T,0.4 V). At low voltage, the period doubling is not visible because successive peaks overlap. At high voltage, we also observe that the first period-doubling tends to be less and less visible: this is due to the loss of resolution at high voltage.

VII. CONCLUSION

There are of course significant uncertainties in the precise values of the experimental parameters. The values of m and $\mathcal{R}$ can drift as a function of voltage. The applied voltage V is not exactly equal to FL. This is only of minor importance. It can only slightly and smoothly distort the plot in Fig. 5(b), i.e., displace the period-doubling regions, but not affect their existence. The shape of the line profiles provides a valuable check on these parameters: e.g., the observation that the symmetric bifurcation profile tends to follow a linear rather than a parabolic locus at higher voltages may be due partly to an increase in effective mass with voltage. The calculations presented here reproduce the detailed features of the experiments. We conclude that our simple dynamical models, using a tunneling model which is device independent—it does not depend on the barrier shapes, heights or details of the tunneling—permit a quantitative analysis of periodic orbit oscillations observed in the RTD.

We thank P. Dando and J. Zakrzewski for helpful discussions. T.S.M. acknowledges funding from EPSRC and thanks the Institute Henri Poincaré in Paris for its hospitality. CPU time has been provided by IDRIS. Laboratoire Kastler-Brossel, de l'Ecole Normale Supérieure et de l'Université Pierre et Marie Curie, is unité associée 18 du CNRS. A.J.F. acknowledges funding from EPSRC.

[1] G. Muller, G. S. Boebinger, H. Mathur, L. N. Pfeiffer, and K. W. West, Phys. Rev. Lett. **75**, 2875 (1995).

[2] G. S. Boebinger, G. Muller, H. Mathur, L. N. Pfeiffer, and K. W. West, Surf. Sci. **361-362**, 742 (1996).

[3] T. M. Fromhold *et al.*, Phys. Rev. Lett. **72**, 2608 (1994).

[4] D. L. Shepelyansky and A. D. Stone, Phys. Rev. Lett. **74**, 2098 (1995); E. Narimanov and A.D. Stone (unpublished).

[5] T. S. Monteiro and P. A. Dando, Phys. Rev. E **53**, 3369 (1996).

[6] P. B. Wilkinson, T. M. Fromhold, and L. Eaves, Nature (London) **380**, 608 (1996).

[7] H. Friedrich and D. Wintgen, Phys. Rep. **183**, 37 (1989).
[8] J. Bardeen, Phys. Rev. Lett. **6**, 57 (1961).
[9] M. Kuś, F. Haake, and D. Delande, Phys. Rev. Lett. **71**, 2167 (1993).
[10] M. C. Gutzwiller, *Chaos in Classical and Quantum Mechanics* (Spinger-Verlag, New York, 1990).
[11] A. M. Ozorio de Almeida and J. H. Hannay, J. Phys. A **20**, 5873 (1987).
[12] W. Miller, J. Chem. Phys. **63**, 996 (1975).